

1 Article

# 2 Deep Learning Model for Magnetic Resonance 3 Imaging Brain Tumor Recognition

4 Abir Fettah<sup>1</sup>, Bouchra Goumidi<sup>1</sup> and Mostafa El Habib Daho<sup>1,\*</sup>

5 <sup>1</sup> Biomedical Engineering Laboratory, University of Tlemcen, Algeria;

6 \* Correspondence: mostafa.elhabibdaho@univ-tlemcen.dz

7 Received: date; Accepted: date; Published: date

8 **Abstract:** Human interpretation of a large quantity of Magnetic Resonance Imaging (MRI images)  
9 is a tiring task and depends on the practitioner's expertise and experience. Glioma is one of the most  
10 common and dangerous types of primary brain tumors, and its early diagnosis could be life-saving.  
11 Precise and fully automatic classification of Glioma on MRI images helps physicians diagnose and  
12 monitor patients.

13 In this work, we propose an automatic system to aid in diagnosing Glioma by classifying brain  
14 tumors into two categories: High-Grade Glioma (HGG) and Low-Grade Glioma (LGG). To perform  
15 this task, we trained three deep learning models (VGG-16, ResNet-50, and Inception-V3) on four  
16 brain MRI datasets (one for each MRI modality). To further improve tumor classification, non-  
17 tumorous slices were removed from the HGG class of the selected dataset and then were separately  
18 used to train the three models. Evaluations on BraTS 2019 attest that T1 presents the most  
19 discriminative features with 0.9513, 0.907, and 0.9487 for accuracy, sensitivity, and specificity,  
20 respectively. The Inception-V3 model outperforms the other models with 0.9975, 0.9894, and 1  
21 for accuracy, sensitivity, and specificity. Experimental results demonstrate that using the Inception-V3  
22 model with T1 modality can achieve good performances.

23 **Keywords:** Glioma, MRI, Deep Learning, Brain Tumor classification, CNN, LGG, HGG.

24

## 25 1. Introduction

26 The brain is one of the foremost complex organs within the human body that works with billions of  
27 cells. Sometimes, these cells can be exposed to an uncontrolled cell division and formed an abnormal  
28 group of cells around or inside the brain; that's what we call brain tumors. This kind of tumor can  
29 affect the traditional functionality of brain activity and cause many problems.

30 Cerebral tumors are classed to benign tumors or low-grade (grade I and II) and malignant tumors  
31 or high-grade (grade III and IV) according to the World Health Organization (WHO) [1]. Some  
32 benign brain tumors are Gliomas (low-grade Gliomas LGG), and most malignant brain tumors are  
33 Gliomas (high-grade Gliomas HGG).

34 Due to the considerable progress in medical image acquisition devices comprises different  
35 modalities and processes, including Magnetic Resonance Imaging (MRI), Computed Tomography  
36 (CT), Positron Emission Tomography (PET) [2], among others, the medical data is quite voluminous.  
37 With the provision of comprehensive information and the support of multimodal MRI brain images,  
38 doctors can perform quantitative analyses of brain tumors such as the diameter, volume, and  
39 maximum amount of brain lesions, which allows the development of a diagnosis and optimal  
40 treatment plan for patients.

41 This manual brain tumor diagnosis is often painstaking. It requires significant and tedious efforts  
42 on the medical expert that can be highly subjective, evaluations and prognoses can be slow [3]. This

43 focuses on the advanced deep learning algorithms that can play a pivotal role in supporting  
44 clinicians in detecting different forms of tumors. A commonly used deep learning method for image  
45 segmentation and classification is to train a Convolutional Neural Network (CNN).

46 In this work, we propose an accurate and fully automatic system for classifying brain tumors into  
47 two classes High-Grade Glioma (HGG) and Low-Grade Glioma (LGG) from volumetric 3D  
48 Magnetic Resonance Imaging (MRI). The trained three well-known architectures, VGG-16, ResNet-  
49 50, and Inception V3, on four converted datasets (T1, T1ce, T2, and FLAIR) to select the most  
50 informative modality which presents more specific features and information to distinguish between  
51 LG and HG gliomas, passing by image pre-processing and data augmentation. Furthermore, non-  
52 tumorous slices in both HGG and LGG classes can lead to false negatives in the predicted output  
53 results. Therefore these slices were removed from the HGG class of the selected dataset, and then  
54 the three models were trained on this pre-processed dataset. Finally, we have proposed an  
55 algorithm that classifies the whole volume using just one modality with the accurate model.

56 The remaining paper is as follows: section 2 provides a summary of the current state-of-the-art in  
57 automated brain tumor classification and segmentation, section 3 introduces the proposed method,  
58 section 4 reports and discusses experimental results performed using the BraTS 2019 database. The  
59 last section includes the conclusion of this work.

## 60 2. Related work

61 Nowadays, brain tumors are among the most dangerous, rapidly growing types of cancer and  
62 deadliest diseases. Specialists try to use different technics for detecting these tumors and localizing  
63 them (manually). Its performance depends on pathologists' experience, and this did not help so  
64 much due to long time consumption and human errors.

65 Researchers pay attention to deep learning and its great performance in image classification and  
66 segmentation; due to their self-learning and generalization ability using large amounts of data.

67 Over the last ten years, many researchers have focused on the segmentation and classification of  
68 tumors on MRI images of the brain, particularly with data availability through the Brain Tumor  
69 Segmentation (BraTS) Challenge. Since this database's appearance in 2012, many researchers have  
70 contributed to the segmentation and classification of the different versions of this database.

71 Among the most recent works, Gonbadi et al. [4] preprocessed two databases, IXI dataset (refers to  
72 normal brains) and BraTS 2017(refers to glioma brain tumors), with the aim of classifying Glioma  
73 Brain Tumors by extracting the brain from the skull using Brain Extraction Tool (BET). They use  
74 CNN model built by gathering several layers (Convolution, Max-pooling, Up-sampling, Dense) to  
75 extract high level and low-level features from input images and finally classify them to three  
76 categories: HGG, LGG or normal brain. In the end, they got a desirable accuracy of 99.18%.

77 In 2019, Linmin Pei et al. [5] suggested a method for brain tumor classification which composed of  
78 two parts: the first use a 3D deep neural network for brain tumor segmentation on the multimodal  
79 magnetic resonance images, and the second part use also a 3D deep neural network that is  
80 developed for tumor classification using tumor segmentation results. Their paper applied their  
81 model on a dataset of Computational Precision Medicine: Radiology-Pathology Challenge (CPM:  
82 Rad-Path) for Brain Tumor Classification 2019. They obtained a dice score of 0.749 and an F1score  
83 of 0.764 for the validation data, while 0.596 for the dice score and 0.603 for the F1score in the test  
84 phase.

85 In [6], the authors proposed for the tumor segmentation task a Fully Convolutional Neural Network  
86 (FCNN) with three-layer deep encoder-decoder architecture is used along with dense connection at  
87 the encoder part. They have performed pre-processing using Z score normalization on individual  
88 MR sequences and data augmentation by rotation, flip, elastic transformation, shear, shift, and zoom  
89 on MRI sequences. The network training on BraTS 2019 uses the focal loss function. Initially, the  
90 network trains on the whole tumor, and then its weights are transfer to substructure network

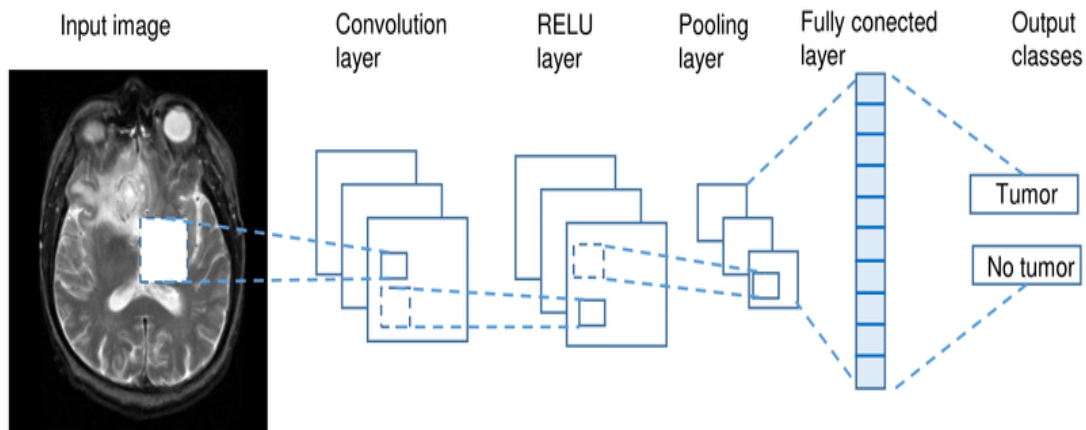
91 training. Radiomic features from the segmentation results, age, and statistical features are used to  
92 predict patients' overall survival using random forest regressors. They obtained a dice similarity of  
93 training dataset with focal loss implementation for whole tumor, tumor core, and enhancing tumor  
94 is 0.92, 0.90, and 0.79, respectively. The overall survival prediction method outperformed the other  
95 methods with 58.6% accuracy for the validation dataset on the leaderboard and the test set of BraTS  
96 2019 with 57.9% accuracy.

97 In the work of Alqazzaz et al. [7], the authors proposed a fully convolutional neural network SegNet  
98 to segment the entire tumor volume and accurately segment the tumor into four sub-tumor parts.  
99 Their work has four main steps: a pre-processing step, in which N4ITK bias field correction is  
100 applied to all MRI modalities, a training step to fine-tune separately four pre-trained SegNet models  
101 with 3D data sets with Flair, T1, T1ce, and T2 modalities as input data, a post-processing step to  
102 extract four maximum feature maps from the SegNet models' score maps, for the last step these  
103 feature maps are combined with the pixel values of the original MRI models, and they are taken as  
104 the input to a dataset classifier to further classify each pixel. Experimental results demonstrate that  
105 this method has the potential to perform well on brain tumor segmentation. Evaluating on BraTS  
106 2017, F-measure scores give 0.85, 0.81, and 0.79 for whole tumor, tumor core, and enhancing tumor,  
107 respectively.

108 In more recent work, Mzoughi et al. [8] proposed a pre-processing technique based on intensity  
109 normalization and adaptive contrast enhancement of MRI data, and they applied a Deep Multi-Scale  
110 3D Convolutional Neural Network on Brats 2018 dataset to classify Gliomas brain tumors into two  
111 classes: HGG and LGG. The proposed method offers an overall accuracy of 96.49% using the  
112 validation dataset.

### 113 3. Methods

114 In a human's life routine, the brain functions work continued through billions of interconnected  
115 neurons. This is the power of the human brain and the reason to imitate its general idea of working  
116 by building a network of interconnected artificial neurons, to perform several tasks like data  
117 processing, object detection, speech recognition, language translation, and decision making.  
118 Some of these neural networks are built with many parameters and layers (more than five layers),  
119 which means we are talking about deep learning (DL). DL is the best solution for dealing with a large  
120 volume of data because its networks are modeled on similar human brain networks.  
121 Deep learning (DL) is a subfield of machine learning (ML), and artificial intelligence (AI) concerned  
122 with algorithms driven by the structure of the brain and mimic the way humans analyzing, collecting,  
123 and interpreting knowledge. It is one of the important data science elements, which makes processing  
124 data and creating patterns for use in decision making faster and easier [9] [10]. Its networks capable  
125 of learning with and without human supervision (learn from labeled and unlabeled data).  
126 For supervised learning tasks, deep learning methods eliminate feature engineering by translating  
127 the data into compact, intermediate representations akin to principal components and derive layered  
128 structures that remove redundancy in representation. The best-known architectures in supervised  
129 learning are the Convolution Neural Network (CNN). This type of neural network is trained by using  
130 big data and owns the capability of extracting features from data via convolutions without manual  
131 extraction of features. It comprises several kinds of layers: an input layer, an output layer, and hidden  
132 layers. The hidden layers consist of convolutional layers, ReLU layers, pooling layers, and fully  
133 connected layers, as is presented in Figure 1. Convolution neural network is one of the most popular  
134 deep learning architectures used for the classification and recognition of image, text, and sound [11]  
135 [12].



136

137

**Figure 1.** High-level general CNN architecture [11]

138

139

In this work, we have used three well-known and widely used architectures in the literature: VGGNet (VGG16), ResNet50, and InceptionV3.

140

141

142

*3.1. VGGNet:* This architecture was introduced by the Visual Geometry Group (Oxford University), VGG [13] is a Convolutional Neural Network architecture based on AlexNet. There are two architectures of VGG: VGG16 & VGG19. The architecture contains:

143

144

145

146

147

148

149

150

151

- Input: VGG used RGB image in a 224x224 pixel.
- Convolutional Layers: In VGG, the convolutional layers use a very small receptive field 3x3. There are also 1x1 convolution filters, which can be seen as a linear transformation of the input channels, followed by a ReLU layer. The convolution stride is fixed to 1 pixel.
- Max Pooling: is performed over a 2x2 pixel window.
- Fully-Connected Layers. VGG contained three fully-connected layers.
- Hidden Layers: All hidden layers are equipped with the non-linearity layer (ReLU). Not all networks contain Local Response Normalisation (LRN) due to their memory and time consuming and does not improve the performance.

152

153

154

VGG16 contained 16 layers (13 convolutional layers + 3 fully connected layers); it is very used due to its uniform Architecture. In the community of extracting features from images, VGG16 is one of the most preferred networks.

155

156

157

158

159

*3.2. ResNet:* Deeper networks can provide more complex features, increasing the robustness and performance of the model. However, adding more layers to the network does not work by simply stacking layers together. Deeper neural networks are difficult to train because of vanishing and exploding gradient types of problems. ResNet [14], one of the common architectures of CNN, allowed us to train extremely deep neural networks.

160

161

162

163

164

Residual Networks 'ResNets' are nearly similar to networks with layers of convolution, pooling, activation, and fully-connected layers. The basic building block for ResNets is the convolutional and identity blocks, which connect the output of one layer with the input of an earlier layer (skip connection). There are many variants of the ResNet architecture depending on the number of layers, such as ResNet-50, ResNet-101, ResNet-110, and ResNet-152.

165

166

167

168

169

170

171

172

173

The architecture of ResNet-50 consists of 5 stages. Every ResNet architecture carries out the initial convolution and max-pooling using 7x7 and 3x3 kernel sizes, respectively. Each convolution block has three convolution layers, and each identity block also has three convolution layers. The network also has an Average Pooling and a fully connected layer with 1000 neurons (ImageNet class output).

174

*3.3. Inception network:* It is a convolutional neural network (CNN) characterized -in addition to its common layers- by its unique module, "Inception module", which was designed to solve the problem of computational expense and overfitting, among other issues. In general Inception network is one of the possible solutions for computer vision problems. The popular versions of inception networks are as follows:

- 175 • Inception v1 or GoogLeNet
- 176 • Inception v2 and Inception v3.
- 177 • Inception v4 and Inception-ResNet.

#### 178 **Inception module:**

179 The inception module combines convolution layers with different filter sizes (5X5, 3X3, 1X1) and max  
 180 pooling. It has a bottleneck layer (1X1 convolutions) used for dimensionality reduction, then  
 181 concatenate all of their output into a single output vector to form the input of the next layer. The  
 182 object from the convolutions of different sizes is to capture details at varied scales [15].

#### 183 **Inception v3:**

184 Inception V3 [16] is the 3rd version of inception architectures characterized by additional  
 185 factorization ideas.

186 Inception V3 is a widely used model for image recognition; this model comprises multiple blocks,  
 187 including convolutions, average pooling, max pooling, concatenations, dropouts, and fully connected  
 188 layers and using the Batch norm to activate inputs also the Softmax to compute the Loss.

189 In this study, we have performed a transfer learning on the VGG16, ResNet-50, and InceptionV3 by  
 190 reusing the weights from the pre-trained models on the ImageNet dataset.

191

## 192 **4. Results and Discussions**

193 In this study, we are interested in the classification of brain tumors into two classes (LGG and HGG).  
 194 We will first test three well-known architectures on the BraTS dataset to perform this task, then  
 195 perform a dataset pre-processing, after that image classification, and finally a full volume  
 196 classification.

197

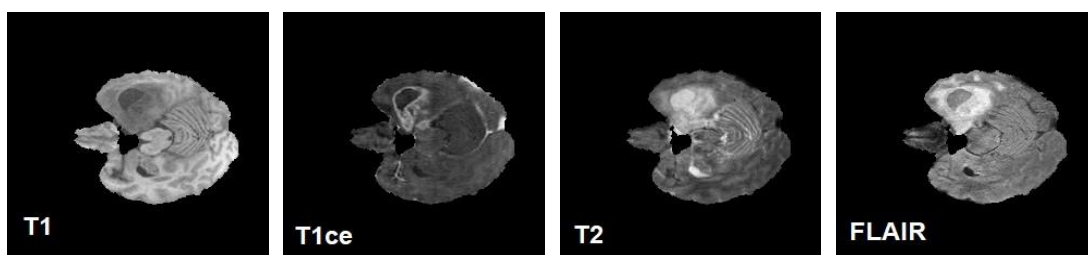
### 198 *4.1. Used dataset:*

199 BraTS utilizes multi-institutional pre-operative MRI scans and primarily focuses on the segmentation  
 200 (Task 1) of intrinsically heterogeneous (in appearance, shape, and histology) brain tumors, namely  
 201 gliomas. Furthermore, to pinpoint this segmentation task's clinical relevance, BraTS also focuses on  
 202 predicting overall patient survival (Task 2) and intends to classify volumes in HGG and LGG classes  
 203 (Task 3). All BraTS multimodal scans (volumes from 335 patients: 259 HGG and 76 LGG volumes)  
 204 are available as NIfTI files (.nii.gz) and were acquired with different clinical protocols and various  
 205 scanners from multiple institutions.

206 BraTS contains four modalities: a) native (T1) and b) post-contrast T1-weighted (T1Gd), c) T2-  
 207 weighted (T2), and d) T2 Fluid Attenuated Inversion Recovery (T2- FLAIR) volumes.

208 All the imaging datasets have been segmented manually,

209 One to four ratings, following the same annotation protocol, and their annotations were approved by  
 210 experienced neuro- radiologists [17]. To train and test our classification model, we have selected a  
 211 subset from the BraTS dataset and divided it into four databases, one for each modality. Each  
 212 modality from the previous four databases contains 155 slices for one patient; in this paper, we will  
 213 work with these slices as PNG images. The used databases provided as a set of slices contain 2015  
 214 High-Grade Glioma (HGG) and 2015 Low-Grade Glioma (LGG) images from the T1, T1ce, T2, and  
 215 FLAIR modalities, respectively. The examples of High and Low-Grade Glioma obtained by T1, T1ce,  
 216 T2, and FLAIR modalities are shown in Figures 2 and 3.



217

218

**Figure 2.** HGG images

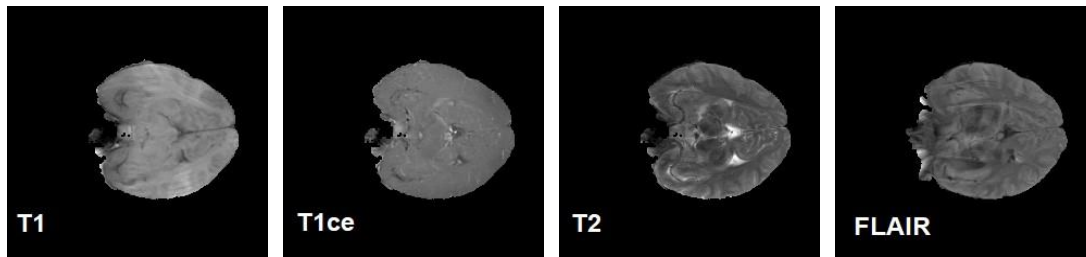


Figure 3. LGG images

#### 4.2. Modality selection

As mentioned before, the BraTS database contains four modalities (T1, T2, T1ce, and FLAIR). This study aims to select the best modality that contains the best information for the classification of brain cancer. Such a study allows us, in the future, to acquire only the most informative modality and thus reduce the cost of MRI.

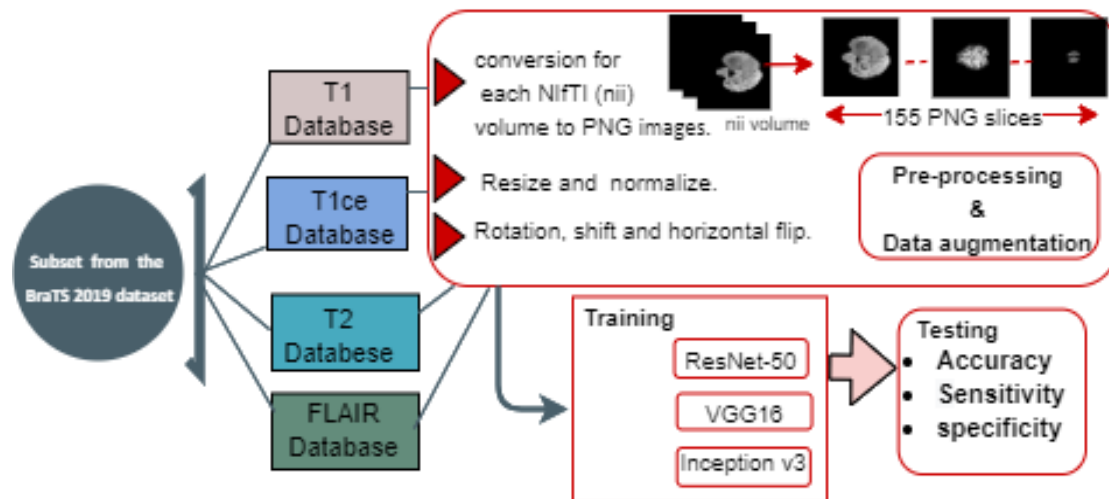


Figure 4. Block diagram: the process of the selection of the database which allows the models to train well.

As shown in Figure 4, we have converted each NIfTI (nii) volume to PNG images; thus, each volume gives us 155 PNG images. We have normalized and readjusted all images' sizes to use them with the deep learning models ( $224 \times 224$  for VGG16 and ResNet50 and  $299 \times 299$  for InceptionV3). To augment the datasets, we transformed each image by rotation, shift, and horizontal flip.

Brain tumor classification was performed using a set of CNN models developed using Keras and Tensorflow on a local machine with a 4820k i7 processor, 56 GB RAM, 8 GB GTX1070 GPU, and Windows 10 operating system.

The classification was achieved using transfer learning on three pre-trained models on the ImageNet database: VGG16, ResNet50, and Inception v3; and BraTS 2019 database divided into four databases for each modality. All the models were trained for 50 epochs using a batch size equal to 16 with an SGD optimizer to minimize the loss function.

Firstly, we applied the chosen models on the first version of our databases (4 datasets without pre-processing) to find which modality helped them train well. The results of this training are shown in Table 1, where Equations (1), (2), and (3) show how to compute specificity, sensitivity, and accuracy, respectively:

$$\text{Specificity} = (\text{TN}) / (\text{TN} + \text{FP}) = \text{Probability of being test negative when disease absent}, \quad (1)$$

$$\text{Sensitivity} = (\text{TP}) / (\text{TP} + \text{FN}) = \text{Probability of being test positive when disease present}, \quad (2)$$

$$\text{Accuracy} = (\text{TN} + \text{TP}) / (\text{TP} + \text{FN} + \text{TN} + \text{FP}), \quad (3)$$

247 With:

- 248 – True Positive (TP) is the number of positive predicted cases and they are actually positive.
- 249 – True Negative (TN) is the number of negative predicted cases and they are also actually negative.
- 250 – False Negative (FN) is the number of negative predicted cases while they are actually positive.
- 251 – False Positive (FP) is the number of positive predicted cases while they are actually negative.
- 252

253 **Table 1.** The calculated performances of the three models applied on four databases.

Dataset	Model	Accuracy	Sensitivity	Specificity
T1CE	Resnet50	0.9413	0.8894	0.9925
	VGG16	0.9438	0.8945	0.9925
	InceptionV3	0.9488	0.8995	<b>0.9975</b>
Flair	Resnet50	0.9437	0.8944	0.9925
	VGG16	0.9474	0.8969	<b>0.9975</b>
	InceptionV3	0.9487	0.8994	<b>0.9975</b>
T1	Resnet50	<b>0.9513</b>	<b>0.907</b>	0.9487
	VGG16	0.9413	0.8894	0.9925
	InceptionV3	0.95	0.9045	0.995
T2	Resnet50	0.9475	0.8969	<b>0.9975</b>
	VGG16	0.9424	0.8944	0.99
	InceptionV3	0.9463	0.8969	0.995

254

255

256 Table 1 summarizes the results obtained by three models learned on four databases (T1, T2, Flair, and  
 257 T1CE without pre-processing). We noticed a difference in the performance of models in terms of  
 258 accuracy, sensitivity, and specificity. In general, diagnostic support systems depend on metrics to  
 259 measure how well they predict the outcomes; one of the important metrics is sensitivity.

260 The higher value of sensitivity means a lower value of false negative. In other words, patients who  
 261 are unhealthy and got predicted as healthy. For that in Brain tumors classification, this metric is  
 262 highly important and puts the focus on it. Based on sensitivity values, we can compare the obtained  
 263 results in training on each dataset to find the one that will give the best generalization also the best  
 264 performance with these models, so this database is the T1 database.

265 One of the major challenges in the converted volumes to 155 PNG images is non-tumorous slices in  
 266 both HGG and LGG classes. These slices can lead to a wrong classification in the predicted output  
 267 results.

268 Secondly, we initiated training with the preceding models on the T1 pre-processed database.

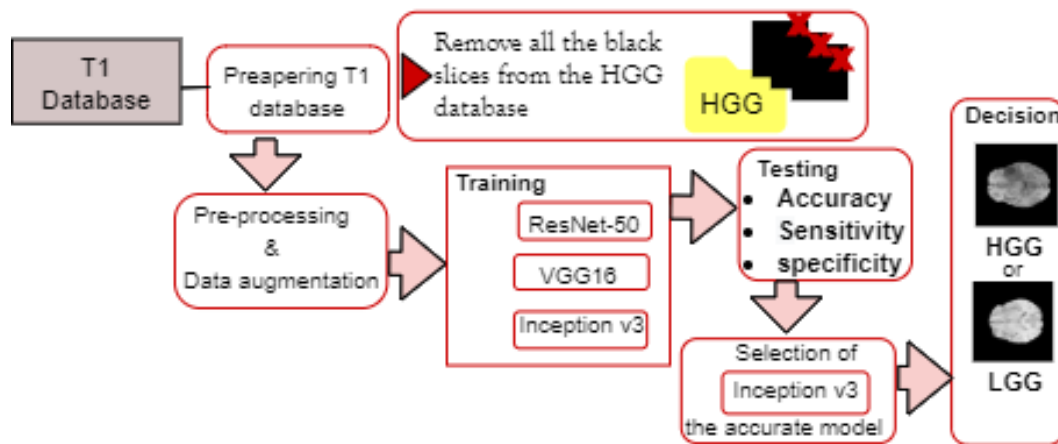
269

#### 270 4.3. Brain tumor image classification

271

272 We have noticed that the volume of HGG contains some black slices, which are also found in LGG  
 273 volumes. To avoid misclassifying these images, since they do not contain any information, we have  
 274 removed them from the HGG database. Such an action will allow us to consider all black slices as

275 LGG and reduce the error rate. The obtained results with this pre-processing step are shown in  
 276 Table2. The same models (VGG16, ResNet50, and Inception V3) were applied on the T1 pre-processed  
 277 dataset (see Figure 5) to select the best model for this pre-processed modality.



278

279 **Figure 5.** Block diagram: the process of the selection of the best model for the T1 pre-processed  
 280 database.

281

282 **Table 2.** The obtained results of performances of training three models on pre-processed T1 dataset.

Dataset	Model	Accuracy	Sensitivity	Specificity
T1 pre-processed	Resnet50	0.9971	0.9876	0.9937
	VGG16	0.9954	0.9805	1
	InceptionV3	<b>0.9975</b>	<b>0.9894</b>	<b>1</b>

283

284

285 According to the found results and the ranking of models based on their performances in Table 2,  
 286 Inception v3 exceeds the others regarding the highest values of precision, sensitivity, and specificity.  
 287 This overall improvement of the results can be explained by the fact that removing the black slices  
 288 has allowed the model to focus on the images that contain relevant information and remove the  
 289 classification error for these black images since they were previously included in both classes.

290 The final objective of this work is to classify the volumes in HGG and LGG; for this, we proposed a  
 291 solution to realize this task.

292

#### 293 4.4. Volume classification

294 Algorithm 1 presents the process of classifying a total volume for one patient that used only one  
 295 modality (T1 with the conversion from nii volume to 155 slices PNG images) from the whole volume.  
 296 The Inception V3 model classifies each image, and at the same time, a counter is increasing if the class  
 297 was HGG; if it is an LGG image, the counter will not be increased. The counter will be tested if at  
 298 least one image is classified as HGG class, which means the patient has an HGG tumor; if not (counter  
 299 =0), that means the patient has an LGG tumor.

300 We have used this algorithm to validate our results on ten volumes (5 HGG and 5 LGG). We obtained  
 301 a classification rate of 100% (all ten volumes were well classified) with an average certainty rate close  
 302 to 95%. These results confirm that physicians can trust our application for potential use in brain  
 303 cancer diagnosis.

304 We also proposed in this work a web application to deploy our model and facilitate its use by  
 305 physicians.

306  
 307  
 308  
 309  
 310  
 311  
 312  
 313  
 314  
 315  
 316  
 317  
 318  
 319  
 320  
 321  
 322  
 323  
 324  
 325  
 326  
 327  
 328

---

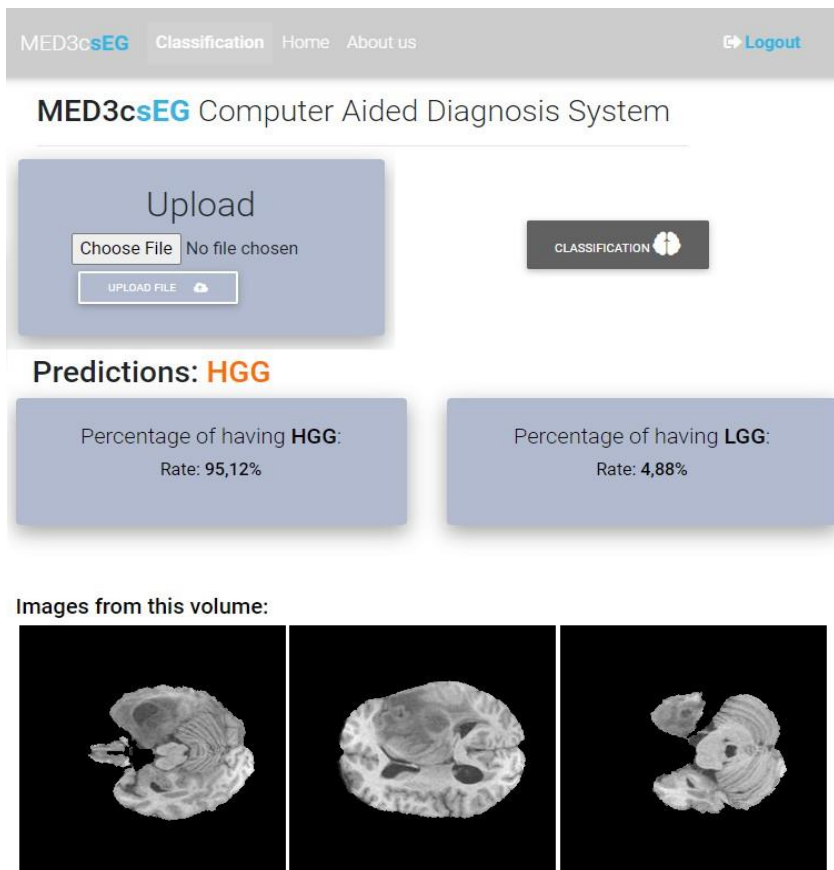
**Algorithm 1: Brain Tumor classification**

---

**Data:** Brain MRI volume (T1 modality) **MRI**  
**Result:** Decision (HGG or LGG) **D**  
 initialization:  $i=0$ ;  
 IMG = decomposition(MRI);  
**for each IMG do**  
      $cl = \text{classify(IMG)}$ ;  
     **if**  $cl == \text{'HGG'}$  **then**  
          $i++$ ;  
     **end**  
**end**  
**if**  $i > 0$  **then**  
      $D = \text{'HGG'}$ ;  
**else**  
      $D = \text{'LGG'}$ ;  
**end**

---

In this application (see Figure 6), the physician, after authentication, loads the T1 volume of the MRI. This volume will be decomposed into 155 PNG images. These images will be classified using our Inception V3 model.



329  
 330

**Figure 6.** Our proposed web application

331 Our web application will help doctors to make decisions. Indeed, at the end of the classification, a  
332 label will be affected to the 3D volume and displayed with a degree of precision and a sample of the  
333 images that contributed to this decision.

## 334 5. Conclusions

335 Brain tumors affect the human's life improperly because of the abnormal growth of cells inside the  
336 brain. It may disturb brain function and be dangerous and life-threatening. Brain tumors are grouped  
337 into two categories benign tumors and malignant tumors. One of the different types of medical  
338 imaging technologies based on a non-invasive approach is MRI that offers greater contrast images -  
339 especially of the brain- that provides different information about the shape or function of organs in  
340 the patient's body. Doctors base their decisions on this information, but unfortunately, this kind of  
341 data is extremely difficult to exploit quantitatively and objectively. In this work, our proposed  
342 approach aims to help the doctor by classifying MRI volumes into two classes HGG and LGG. First,  
343 we have performed a decomposition of each modality (T1, T2, T1ce, and Flair) of the MRI volumes  
344 to 155 PNG images. These images were used to train and test three well-known CNN architectures  
345 in the state-of-the-art. This experiment aimed to choose the best modality in the classification of  
346 brain tumors. The results show that the T1 gives the best performances. We have noticed that the  
347 LGG and HGG volumes contain black slices, leading to misclassification. To solve this problem, we  
348 have proposed to delete these images from the HGG dataset. This pre-processing step allowed the  
349 model to increase the accuracy rate using the Inception V3, and it obtains 0.9975, 0.9894, and 1 for the  
350 accuracy, sensitivity, and specificity, respectively. Finally, we have proposed an algorithm that  
351 classifies the whole volume. Based on the obtained results, we can conclude that such a system will  
352 be of great use to radiologists in helping to diagnose brain cancer.

353

354 **Acknowledgments:** The authors would like to thank the Directorate-General of Scientific Research and  
355 Technological Development (Direction Générale de la Recherche Scientifique et du Développement  
356 Technologique, DGRSDT, URL: [www.dgrsdtdz.dz](http://www.dgrsdtdz.dz), Algeria) for the financial assistance towards this research.

## 357 References

- 358 1. D. N. Louis, A. Perry, G. Reifenberger, A. Von Deimling, D. Figarella-Branger, W. K. Cavenee, H. Ohgaki,  
359 O. D. Wiestler, P. Kleihues, and D. W. Ellison, "The 2016 world health organization classification of tu-  
360 mors of the central nervous system: a summary," *Acta neuropathologica*, vol. 131, no. 6, pp. 803–820, 2016.
- 361 2. M. D. Guimaraes, J. Noschang, S. R. Teixeira, M. K. Santos, H. M. Lederman, V. Tostes,  
362 V. Kundra, A. D. Oliveira, B. Hochegger, and E. Marchiori, "Whole-body mri in pediatric patients with  
363 cancer," *Cancer Imaging*, vol. 17, no. 1, pp. 1–12, 2017.
- 364 3. D. Shen, G. Wu, and H.-I. Suk, "Deep learning in medical image analysis," *Annual review of biomedical*  
365 *engineering*, vol. 19, pp. 221–248, 2017.
- 366 4. F. B. Gonbadi and H. Khotanlou, "Glioma brain tumors diagnosis and classification in MRI images based  
367 on convolutional neural networks," in *2019 9th International Conference on Computer and Knowledge*  
368 *Engineering (ICCKE)*, 2019, pp. 1–5.
- 369 5. L. Pei, L. Vidyaratne, W.-W. Hsu, M. M. Rahman, and K. M. Iftekharaud- din, "Brain tumor classification  
370 using 3d convolutional neural network," in *International MICCAI Brain lesion Workshop*. Springer, 2019,  
371 pp. 335–342.
- 372 6. R. R. Agravat and M. S. Raval, "Brain tumor segmentation and survival prediction," in *International*  
373 *MICCAI Brainlesion Workshop*. Springer, 2019, pp. 338–348.
- 374 7. S. Alqazzaz, X. Sun, X. Yang, and L. Nokes, "Automated brain tumor segmentation on multi-modal mr  
375 image using segnet," *Computational Visual Media*, vol. 5, no. 2, pp. 209–219, 2019.
- 376 8. H. Mzoughi, I. Njeh, A. Wali, M. B. Slima, A. Ben Hamida, C. Mhiri, and K. B. Mahfoudhe, "Deep multi-  
377 scale 3d convolutional neural network (CNN) for MRI gliomas brain tumor classification," *Journal of*  
378 *Digital Imaging*, 2020.
- 379 9. V. Kumar and M. L., "Deep learning as a frontier of machine learning: A review," *International Journal of*  
380 *Computer Applications*, vol. 182, pp. 22–30, 07 2018.

- 381 10. A. Muniyasamy and A. Alasiry, "Deep learning: The impact on future elearning," *International Journal of*  
382 *Emerging Technologies in Learning (IJET)*, vol. 15, p. 188, 01 2020.
- 383 11. J. Ker, L. Wang, J. Rao, and T. Lim, "Deep learning applications in medical image analysis," *Ieee Access*,  
384 vol. 6, pp. 9375–9389, 2017.
- 385 12. Y. LeCun, Y. Bengio, and G. Hinton, "Deep learning," *nature*, vol. 521, no. 7553, pp. 436–444, 2015.
- 386 13. K. Simonyan and A. Zisserman, "Very deep convolutional networks for large-scale image recognition,"  
387 *arXiv preprint arXiv:1409.1556*, 2014.
- 388 14. K. He, X. Zhang, S. Ren, and J. Sun, "Deep residual learning for image recognition," in *Proceedings of the*  
389 *IEEE conference on computer vision and pattern recognition*, 2016, pp. 770–778.
- 390 15. X.-F. Xu, L. Zhang, C.-D. Duan, and Y. Lu, "Research on inception module incorporated siamese  
391 convolutional neural networks to realize face recognition," *IEEE Access*, vol. 8, pp. 12 168–12 178, 2019.
- 392 16. C. Szegedy, W. Liu, Y. Jia, P. Sermanet, S. Reed, D. Anguelov, D. Erhan, V. Vanhoucke, and A. Rabinovich,  
393 "Going deeper with convolutions," in *Proceedings of the IEEE conference on computer vision and pattern*  
394 *recognition*, 2015, pp. 1–9.
- 395 17. P. Spyridon Bakas, "Multimodal brain tumor seg-  
396 mentation challenge 2020: Data." [Online]. Available: <https://www.med.upenn.edu/cbica/brats2020/data.html>